JACS
JOURNAL OF THE AMERICAN CHEMICAL SOCIETY

Article

pubs.acs.org/JACS

Semiconductor@Metal–Organic Framework Core–Shell Heterostructures: A Case of ZnO@ZIF-8 Nanorods with Selective Photoelectrochemical Response

Wen-wen Zhan, Qin Kuang,* Jian-zhang Zhou, Xiang-jian Kong,* Zhao-xiong Xie, and Lan-sun Zheng

State Key Laboratory for Physical Chemistry of Solid Surfaces & Department of Chemistry, College of Chemistry and Chemical Engineering, Xiamen University, Xiamen 361005, China

Supporting Information

ABSTRACT: Metal–organic frameworks (MOFs) and related material classes are attracting considerable attention for their applications in gas storage/separation as well as catalysis. In contrast, research concerning potential uses in electronic devices (such as sensors) is in its infancy, which might be due to a great challenge in the fabrication of MOFs and semiconductor composites with well-designed structures. In this paper, we proposed a simple self-template strategy to fabricate metal oxide semiconductor@MOF core–shell heterostructures, and successfully obtained freestanding ZnO@ZIF-8 nanorods as well as vertically standing arrays (including nanorod arrays and nanotube arrays). In this synthetic process, ZnO nanorods not only act as the template but also provide Zn^{2+} ions for the formation of ZIF-8. In addition, we have demonstrated that solvent composition and reaction temperature are two crucial factors for successfully fabricating well-defined ZnO@ZIF-8 heterostructures. As we expect, the as-prepared ZnO@ZIF-8 nanorod arrays display distinct photoelectrochemical response to hole scavengers with different molecule sizes (e.g., H_2O_2 and ascorbic acid) owing to the limitation of the aperture of the ZIF-8 shell. Excitingly, such ZnO@ZIF-8 nanorod arrays were successfully applied to the detection of H_2O_2 in the presence of serous buffer solution. Therefore, it is reasonable to believe that the semiconductor@MOFs heterostructure potentially has promising applications in many electronic devices including sensors.

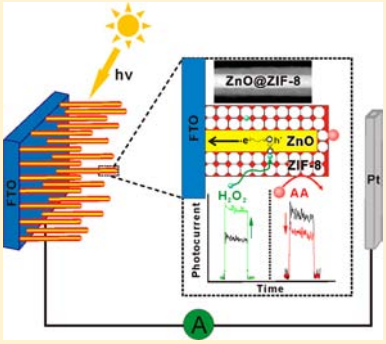

1. INTRODUCTION

Metal–organic frameworks (MOFs) are a class of crystalline inorganic–organic hybrid materials with a well-defined porous structure. Compared with conventional inorganic porous materials, MOFs possess larger porosity and specific surface areas, and especially their pore size and surface functionality can be easily tuned upon selection of different metal ions and organic bridging ligands.[1] Consequently, much attention has been paid to potential applications of MOFs in sensors,[2] catalysis,[3] gas separation,[4] and storage,[5] where MOFs display strong molecule-size-selective ability due to the limitation effect of the pore sizes.

Compared with pure MOFs, the heterostructures integrating MOFs with other functional materials show great advantages due to their synergism effect. For example, embedding-type MOF heterostructures, which are prepared through embedding some metal (e.g., Au, Pd, etc.) and semiconductor (e.g., ZnO and GaN) nanoparticles into the cavities of MOFs, have been demonstrated to exhibit exciting catalytic abilities in heterocatalysis, also with great changes in luminescence and adsorption reaction properties.[6,7] By contrast, researches on MOF core–shell heterostructures with functional materials as core and MOFs as shell have not been popular to date.[8] In fact, the potential multifunctions of MOF core–shell heterostructures are likewise attractive as we can rationally utilize the combination of molecule-size-selective ability of MOFs shell and the application of the core functional material we choose. For example, many metal oxides (such as ZnO) are very important functional materials with semiconducting properties, especially for applications in photoelectrochemistry.[9] Predictably, such semiconductor@MOFs heterostructures should possess potential application in photoelectrochemical (PEC) sensors with a high selective response toward molecules of different sizes.

In the syntheses of the MOF core–shell heterostructures there are two great challenges: (1) how to confine the growth of MOFs to the core surface; (2) how to control shapes of such core–shell heterostructures. The template method is believed to be a very effective strategy for fabricating MOF core–shell heterostructures, by which the size and morphology of the heterostructure can be straightforwardly controlled by the template used. For example, zero-dimensional Fe_3O_4@MOF (e.g., $[Cu_3(btc)_2]$ and MIL-100(Fe)) microspheres and one-dimensional Si@MOF-199 nanowires have been successfully obtained via a versatile step-by-step strategy by using Fe_3O_4 spheres and Si nanowires as templates, respectively.[10] However, the present template methods usually require surface modification with specific functional groups on the template, so as to confine the growth of MOFs on the template surface,

Received: November 14, 2012
Published: January 3, 2013

   dx.doi.org/10.1021/ja311085e | J. Am. Chem. Soc. 2013, 135, 1926–1933

but even so the direct nucleation and growth of MOFs in solution cannot be prevented. By contrast, the self-template synthetic strategy based on metal oxides nanostructures may be a feasible solution,[11] as metal oxide templates can provide metal ions through sacrificing themselves and then initiate the growth of MOFs without any surface modification. As we know, ZnO possesses the richest morphologies at nanoscale (e.g., nanorods, nanobelts, nanotetrapods, nanorings, nanocombs and nanopyramids) among metal oxides.[12] Likewise the Zn^{2+}-MOFs may display the most diversity in crystallography.[13] In this regard, ZnO is regarded as the most suitable model system to explore the fabrication and potential applications of the semiconductor@MOFs heterostructure. In this paper, we successfully fabricated ZnO@zeolitic imidazolate frameworks-8 (ZIF-8) nanorods and nanotubes with core−shell heterostructures, by using a ZnO nanorod and nanotube as sacrificial templates that can provide Zn^{2+} ions for the formation of ZIF-8 by dissolving themselves with the assistance of solvents. Excitingly, the as-prepared ZnO@ZIF-8 nanorod arrays indeed exhibited distinct PEC response toward hydrogen peroxide or ascorbic acid in the electrolyte solution due to the limitation of the aperture of ZIF-8.

2. EXPERIMENTAL SECTION

2.1. Chemicals. Zinc acetate hydrate ($ZnAc_2{\cdot}2H_2O$, 99%), zinc nitrate hexahydrate ($Zn(NO_3)_2{\cdot}6H_2O$, 99%), sodium hydroxide (NaOH, 96%), glycerine (99%), 2-methylimidazole, *N*,*N*-dimethylformamide (DMF, 99.5%), hexamethylenetetramine (HMTA, 99%), hydrogen peroxide (H_2O_2, 30%), and ascorbic acid (AA, 99.7%) were purchased from commercial suppliers (Alfa Aesar and Sinopharm Chemical Regent Co., Ltd.). All chemicals were used as received without further purification.

2.2. Synthetic Procedure. As shown in Scheme 1, ZnO@ZIF-8 nanorods were synthesized with prefabricated ZnO nanorods as sacrificial templates in the mixed solvent of *N*, *N*-dimethylformamide and H_2O. In this strategy, the ZnO nanorods act as the template as well as the Zn source, while 2-methylimidazole acts as the ligand as well as the etching reagent.

Scheme 1. Schematic Illustration of ZnO@ZIF-8 Nanorods Synthesized via the Self-Template Strategy

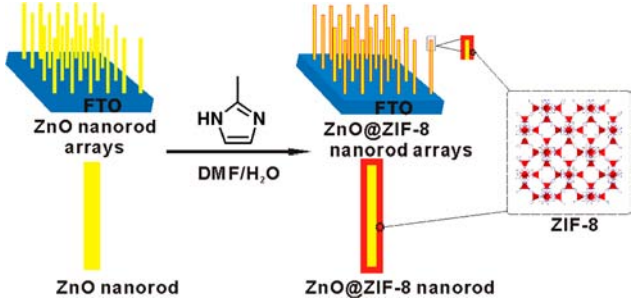

Syntheses of ZnO@ZIF-8 Nanorods. Freestanding ZnO nanorods were synthesized via a hydrothermal route reported in our previous study.[14] Before use, ZnO nanorods were calcined at 500 °C in muffle furnace to remove the surfactants adsorbed on the surface. The growth of ZIF-8 on the ZnO nanorods template proceeded via a simple chemical bath route. In a typical experiment, 2-methylimidazole (0.1650 g, 2 mmol) and ZnO nanorods (0.0204 g, 0.25 mmol) were in sequence added to a Teflon-lined stainless-steel autoclave (25 mL) containing a mixed solvent of DMF/H_2O (16 mL, 3:1 of v/v). After sonication for 5 min, the autoclave was transferred to an oven preheated to 70 °C. After the mixture reacted for 24 h, the white product was collected by centrifugation and washed by fresh DMF and ethanol for several times.

Syntheses of ZnO@ZIF-8 Nanorod (or Nanotube) Arrays. ZnO nanorod arrays were grown on a fluorine-doped tin oxide (FTO) coated glass (2 cm ×1 cm) through galvanostatic electrodeposition for 50 min with a Pt plate as a counter electrode and with an aqueous solution of $Zn(NO_3)_2{\cdot}6H_2O$ (5 mM) and equimolar HMTA as the electrolyte.[15] ZnO nanotube arrays were synthesized by selectively dissolving ZnO nanorod arrays in 0.03 M ethylenediamine with a constant cathode current density of 1.35 $\mu A/cm^2$ and etching charge of about 3.0×10^3 C at a reaction temperature of 70 °C.[16] The FTO substrate grown with ZnO nanorod or nanotube arrays was placed in the Teflon-lined stainless-steel autoclave (25 mL), in which 2-methylimidazole (0.10 g, 1.2 mmol) was dissolved with a mixed solvent of DMF/H_2O (16 mL, 3:1 of v/v). After the mixture was heated in an oven of 70 °C for 24 h, the ZnO@ZIF-8 nanorod (naotube) arrays were obtained and washed by ethanol.

2.3. Structural Characterization and Photoelectrochemical Measurement of the Products. The compositions of the products were acquired by powder X-ray diffraction (XRD, Panalytical X-pert diffractometer with CuKα radiation). The morphologies of the products were observed by a scanning electron microscope (SEM, S4800) and a high-resolution transmission electron microscope (HRTEM, TECNAI F-30) with an acceleration voltage of 300 kV and which was equipped with a Gatan image filtering (GIF) system. Photoelectrochemical (PEC) measurements were carried out in a three-electrode cell with a flat quartz window to facilitate illumination of the photoelectrode surface, which was recorded by a photoelectrochemical system consisting of a potentiostat (model 273a, PAR), a two-phase lock-in amplifier (model 5210, PAR) with a chopper (model 194a, PAR), and a 150 W xenon lamp. In the PEC measurement, the FTO glasses grown with ZnO@ZIF-8 nanorod arrays acted as working electrode with a light intensity of 4.375 mW mm^{-2} and a light area of 8 mm^2 when working. The system also included a platinum wire as auxiliary electrode and saturated calomel electrode (SCE) as reference electrode. The electrolyte consisted of standard phosphate buffer solution (pH = 6.8) and probing molecular species (i.e., H_2O_2 or AA) of different concentrations. The serous buffer solution was composed of standard phosphate buffer solution and serum (3.33% in volume). All the measurements were carried out at the voltage of 0.5 V (vs SCE).

3. RESULTS AND DISCUSSION

3.1. Morphology and Composition of the ZnO@ZIF-8 core−shell nanorods. Figure 1a shows a typical SEM image of the product synthesized with the use of prefabricated ZnO nanorods as the template in the mixed solvent of DMF and H_2O (3:1 of v/v) at 70 °C for 24 h. The product consists of high-purity rodlike nanostructures with 1.5 ± 0.5 μm in diameter, presenting a visible core−shell structure. The powder XRD pattern (Figure 1b) characterization reveals that the product is composed of two kinds of materials with distinct crystal structures. Except for those diffraction peaks assigned to wurtzite-type ZnO (JCPDS no. 36-1451), the residual

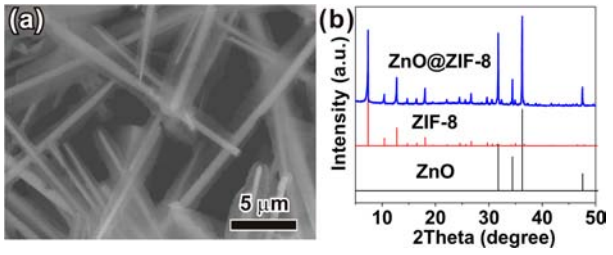

Figure 1. (a) SEM image and (b) XRD pattern of ZnO@ZIF-8 nanorods obtained at 70 °C for 24 h.

dx.doi.org/10.1021/ja311085e | J. Am. Chem. Soc. 2013, 135, 1926−1933

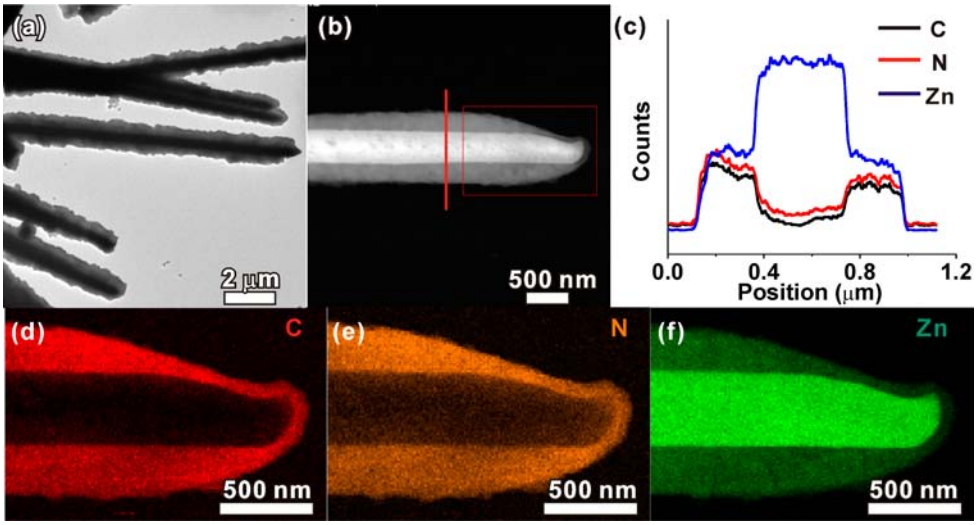

Figure 2. (a) Low-magnification TEM image of ZnO@ZIF-8 nanorods; (b) HAADF-STEM image of an individual ZnO@ZIF-8 nanorod; (c) cross-sectional compositional line profiles of ZnO/ZIF-8 recorded along the line marked in panel b; (d–f) elemental maps of C, N, and Zn concentrations in the ZnO@ZIF-8 nanorod recorded from the zone marked with a rectangle in panel b.

diffraction peaks agree well with the simulated XRD pattern of ZIF-8 with a cubic space group ($I\bar{4}3m$) according to the published crystal structure data.[17]

Figure 2a shows a typical TEM image of the prepared nanorods. Preliminary statistics show that the thickness of the outer shell with light contrast is about 300 ± 25 nm, while the diameter of the inner ZnO nanorods with dark contrast is about 400 ± 25 nm. Note that the ZnO cores are much thinner than the pristine nanorods, which are 600 ± 100 nm in diameter and 15 ± 5 μm in length before reaction (see Supporting Information, Figure S1). Such a core–shell structure is particularly obvious in the high-angle annular dark-field scanning TEM (HAADF-STEM) image (Figure 2b), in which ZnO nanorod as the core appears as brighter contrast due to larger atomic mass. The corresponding cross-sectional composition line profiles (Figure 2c) and element maps (Figures 2d–f) demonstrate that N and C elements mostly locate in the outer layer of the nanorod, while Zn element distributes in the whole nanorod, with relatively higher concentration in the core area. Note that N and C are two main elements of 2-methylimidazole which only exists in the ZIF-8 shell as the ligand. Combined with the XRD results, the above results demonstrate that ZnO@ZIF-8 nanorods with a core–shell structure have been successfully prepared by our proposed self-template method.

3.2. Growth Process of ZnO@ZIF-8 Core–Shell Nanorods. To probe into the growth process of ZnO@ZIF-8 nanorods, time-dependent reactions were further carried out (Figure 3a–d). At the early stage of reaction (i.e., at 4 h), the surface of ZnO nanorods becomes rough and is deposited with some ZIF-8 nanoparticles of 75 ± 25 nm. With prolonged reaction time to 8 h, those ZIF-8 nanoparticles grow up and form a continuous layer on the surface of the ZnO nanorods. At this moment, the thickness of the ZIF-8 layer is about 200 ± 50 nm, whereas the diameter of the ZnO nanorods decreases to 400 ± 25 nm. Herein, the thickness ratio $T_{ZIF\text{-}8}/D_{ZnO}$ ($T_{ZIF\text{-}8}$, the thickness of ZIF-8 shells; D_{ZnO}, the diameter of ZnO cores) is introduced to semiquantitatively depict the evolution degree from ZnO nanorods to ZnO@ZIF-8 nanorods (Figure 3e). The larger $T_{ZIF\text{-}8}/D_{ZnO}$ is, the larger the evolution degree is. The average value of $T_{ZIF\text{-}8}/D_{ZnO}$ for the ZnO@ZIF-8 nanorods

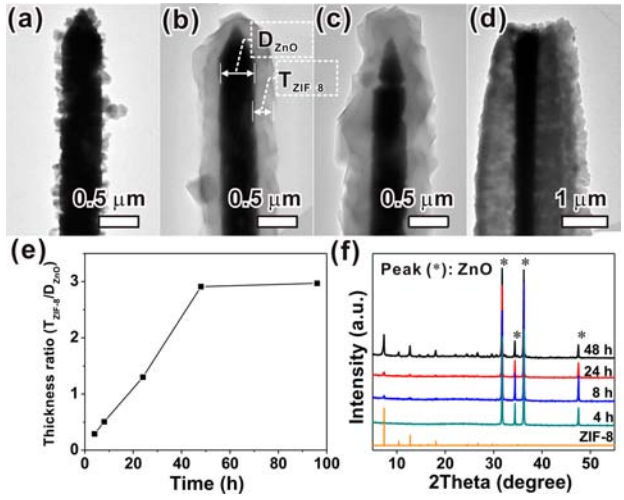

Figure 3. (a–d) Low-magnification TEM images of ZnO@ZIF-8 nanorods obtained after reaction for 4, 8, 24, and 48 h, respectively; (e) thickness ratio ($T_{ZIF\text{-}8}/D_{ZnO}$) and (f) corresponding XRD patterns of ZnO@ZIF-8 nanorods as a function of reaction time.

obtained at 8 h is about 0.51. At 48 h, the average $T_{ZIF\text{-}8}/D_{ZnO}$ ratio reaches 2.9, and accordingly the diameter of the whole ZnO@ZIF-8 core–shell heterostructure increases to 2.5 μm, much larger than that of the pristine ZnO nanorods. As the reaction proceeds, the ZIF-8 shells become thicker and thicker, while the ZnO nanorod cores become thinner and thinner. This phenomenon means that the 2-methylimidazole ligands are able to pass the pores of the ZIF-8 and reach the surface of the ZnO nanorod core where they coordinate with the dissolved Zn^{2+} ions to form ZIF-8, meanwhile, Zn^{2+} ions diffuse outward and react with the ligands at the outer surface of ZIF-8 layer. It should be noted that the $T_{ZIF\text{-}8}/D_{ZnO}$ ratio reaches a relatively constant value after reaction for over 48 h, indicating that the growth of the ZIF-8 shells stops because of the diffusion limitation.

It is necessary to point out that the ZIF-8 shell is very compact, and no pinholes are found during our observation. In addition, no freestanding ZIF-8 nanoparticles are found at any

dx.doi.org/10.1021/ja311085e | J. Am. Chem. Soc. 2013, 135, 1926–1933

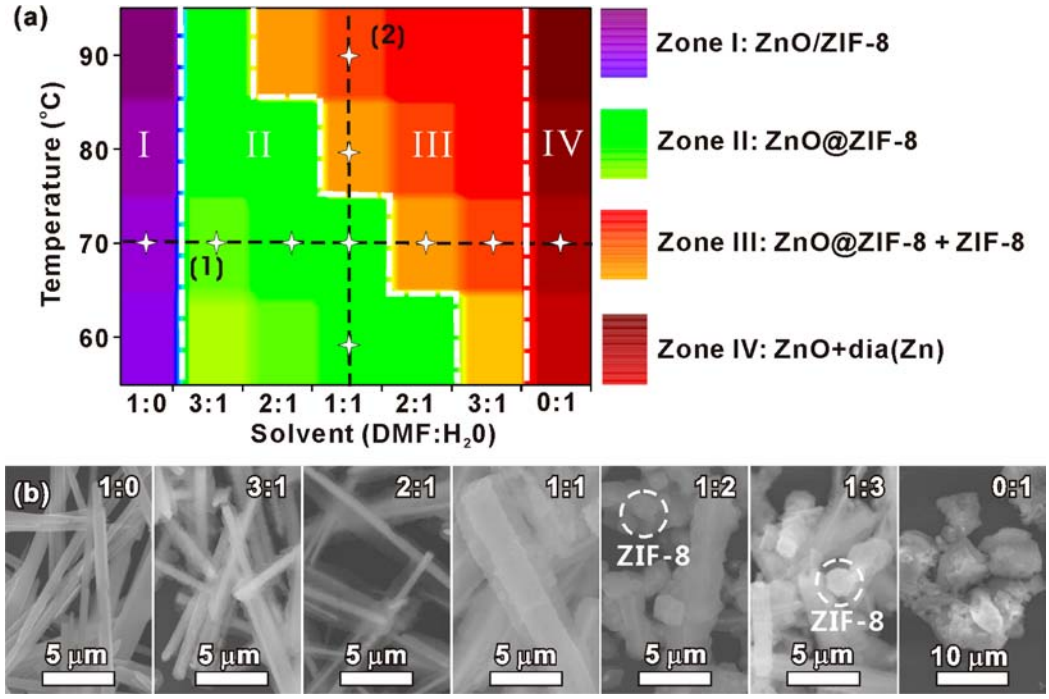

Figure 4. (a) "Phase diagram" that correlates the solvent composition (horizontal ordinate) and reaction temperature (vertical ordinate). Zone I, ZnO coated with ZIF-8; zone II, ZnO@ZIF-8 nanorods with well-defined core−shell structure; zone III, ZnO@ZIF-8 and freestanding ZIF-8; zone IV, ZnO and dia(Zn). The depth of different color represents the content of ZIF-8 (or dia(Zn)) in the products. The lines 1 and 2 correspond to the representative results, respectively, which show effects of the solvent composition and reaction temperature. (b) SEM images of the products obtained with different ratios of solvents at 70 °C (the line 1 marked in phase diagram).

reaction time, suggesting that the growth of ZIF-8 is strictly limited to the surface of ZnO nanorods. The composition and structure changes of the product with the reaction time are reflected in the corresponding XRD patterns as well (Figure 3f). For the product obtained at 4 h, apart from those diffraction peaks assigned to ZnO (marked with an asterisk (∗)), a very weak diffraction peak can be detected at $2\theta = 7.3°$, corresponding to the (011) plane of ZIF-8. As the reaction proceeds, the diffraction peaks belonging to ZIF-8 become stronger and stronger, agreeing with the previous description.

3.3. Influences of the Reaction Conditions on ZnO@ZIF-8 Core−Shell Nanorods. Different from conventional synthetic methods of nano-ZIF-8,[18] no foreign Zn source was used in our proposed method. Therefore, it is assured that Zn^{2+} ions of ZIF-8 originate from ZnO nanorods that are gradually dissolved as the sacrificial template. The growth process of ZIF-8 depends on two factors, the release rate of Zn^{2+} ions and the coordination rate with 2-methylimidazole, both of which are greatly affected by the solvent composition and reaction temperature. In our study, systematic experiments were carried out to illuminate the effects of the solvent composition and reaction temperature. All the experimental results are summarized in the "phase diagram" shown in Figure 4a, which was generated from the results of 28 designed experiments under different conditions (see Figures S2−S5 and Table S1 in Supporting Information). In this phase diagram, the quality of the products is represented by different colors and depths, considering their morphology, composition, and uniformity through SEM, TEM, and XRD. This phase diagram can be briefly divided into four zones: (1) zone I where the products are dominated by ZnO nanorods coated with some ZIF-8 nanoparticles; (2) zone II where the products are high-purity (>95%) ZnO@ZIF-8 nanorods with well-defined core−shell heterostructures; (3) zone III where the products are composed of ZnO@ZIF-8 nanorods and some freestanding ZIF-8 due to the direct nucleation and growth in solution; (4) zone IV where some ZnO nanorods are partially converted into other MOFs, a compound with the dense dia framework (dia(Zn)).[19] Zone II with green color is the optimized synthetic conditions, and the depth of the green correlates the thickness ratio of the ZIF-8 shell to the ZnO core (i.e., the $T_{ZIF\text{-}8}/D_{ZnO}$ ratio). Under these appropriate conditions, the value of $T_{ZIF\text{-}8}/D_{ZnO}$ increases with reaction temperature and the H_2O content in the mixed solvent.

Herein we take the experimental results at 70 °C as an example to expatiate the effect of the solvent composition (Figure 4b, the line (1) in the phase diagram). When DMF is solely used as solvent, no changes occur on the morphology of ZnO nanorods, and XRD characterization confirms the absence of ZIF-8 (see Supporting Information, Figure S3 and Table S1 for detailed results). When H_2O is added into DMF with a certain ratio (i.e., DMF/H_2O = 3:1, 2:1, 1:1), ZIF-8 can grow on the surface of ZnO nanorods, the well-defined ZnO@ZIF-8 nanorods can be obtained, and the $T_{ZIF\text{-}8}$ increases with the content of H_2O in the mixed solvent, whereas the D_{ZnO} decreases accordingly. When the H_2O content further increases (i.e., DMF/H_2O = 1:2 or 1:3), some freestanding ZIF-8 particles are found together with ZnO@ZIF-8 nanorods, as indicated with dashed cycles in SEM images. When H_2O is solely used as solvent, most of the ZnO nanorods are dissolved, and the product is dominated by spherical particles tens of micrometers in size. The XRD pattern reveals that those spherical particles are mainly composed of dia(Zn), instead of ZIF-8. Reaction temperature is another key factor for the formation of ZnO@ZIF-8 nanorods. As indicated by line (2) in the phase diagram, at low reaction temperatures (i.e., 60 and 70

dx.doi.org/10.1021/ja311085e | J. Am. Chem. Soc. 2013, 135, 1926−1933

°C), high-purity ZnO@ZIF-8 nanorods can be formed with the mixed solvent of DMF/H_2O = 1:1 (Supporting Information, Figures S2d, S3d). However, higher reaction temperatures can result in the coexistence of ZnO@ZIF-8 nanorods and freestanding ZIF-8 particles. In the product at 80 °C, the former accounts for 80−90%, while in the product at 90 °C this ratio decreases to 50−60% (Supporting Information, Figures S4d, S5d, and Table S1).

As a kind of amphoteric oxides, ZnO is easily dissolved to release Zn^{2+} ions in acidic or basic aqueous solutions.[20] In our reaction system, 2-methylimidazole plays dual roles, that is, dissolving ZnO nanorods as etching reagent to release Zn^{2+} ions and coordinating with Zn^{2+} ions as ligand to form ZIF-8. The balance between the dissolution rate and the coordination rate is crucial for the formation of well-defined ZnO@ZIF-8 nanorods. When pure water is used as solvent, the pH of the solution is about 9 and the dissolution rate of ZnO nanorods is faster than the coordination rate. Consequently, the coordination process is prone to directly take place in solution rather than on the surface of ZnO nanorods. To slow down the dissolution rate of ZnO, DMF is designedly introduced as solvent in the synthetic process. However, the etching ability of 2-methylimidazole in DMF is too poor to release enough concentration of Zn^{2+} for the formation of ZIF-8. Therefore, the appropriate solvent composition is crucial for successful preparation of well-defined ZnO@ZIF-8 nanorods. Likewise, the temperature has a great influence on the balance between the dissolution rate of ZnO nanorods and the coordination rate with the ligands. In addition, other organic solvents such as DEF (*N*,*N*-diethylformamide) were proved to have the ability of playing the same role as DMF (as shown in Supporting Information, Figure S6).

On the basis of the above growth mechanism, it can be deduced that our proposed self-template strategy should possess good versatility. To prove this, such a self-template synthetic strategy was also applied to the fabrication of ZnO@ZIF-8 nanorod or nanotube arrays. Figures 5a,b show SEM images of ZnO nanorod arrays and nanotube arrays grown on the FTO substrate by electrochemical deposition. The diameter of ZnO nanorods is in the range of 300 ± 25 nm and the length is up to 2−3 μm. Through electrochemical dissolution, those ZnO nanorods can be etched along the [0001] direction and become hollow nanotubes with an internal diameter of about 100−140 nm (Figure 5b). After the chemical bath deposition, both the nanorod arrays and the nanotube arrays can be enclosed with a layer of compact ZIF-8 (Figure 5c,d). The corresponding XRD patterns (Figure 5e) and TEM characterization (Supporting Information, Figure S7) confirm the presence of core−shell heterostructures. Note that in the XRD patterns the diffraction peaks marked with the diamond (♦) originate from the FTO substrate. Similar to that of the freestanding nanorods case, the whole core−shell structure in the nanorod arrays becomes thicker (about 400 ± 50 nm), while the diameter of the ZnO core becomes thinner (about 200 ± 25 nm) (Supporting Information, Figure S7a,c). As to the nanotube arrays, it can be found that the internal diameter of the nanotubes obviously shrinks, up to 80 ± 25 nm, indicating that both sides of the ZnO nanotubes are grown with ZIF-8 (Figure 5d). This phenomenon reveals that using metal oxide as a template can control the nucleation sites by sacrificing themselves providing metal ions.

3.4. Photoelectrochemical Test of the ZnO@ZIF-8 Nanorod Arrays. ZnO is one of the most important

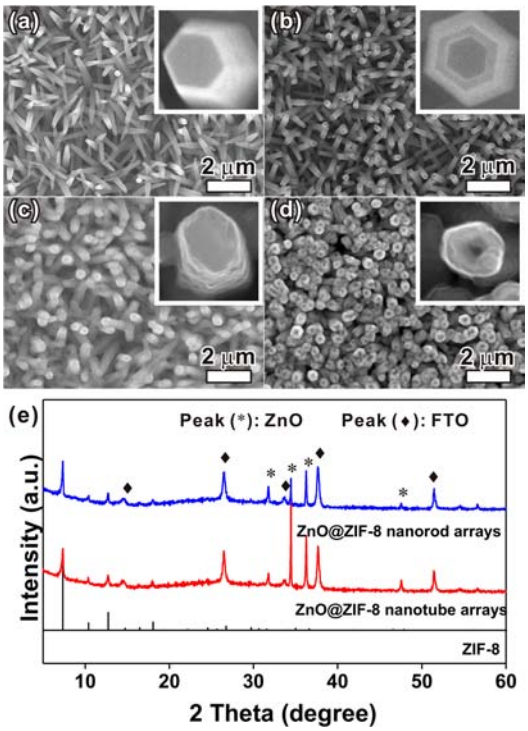

Figure 5. (a,b) Low-magnification and high-magnification (inset) SEM images of the templates, ZnO nanorod and nanotube arrays grown on FTO substrate, respectively. (c,d) Low-magnification and high-magnification (inset) SEM images of the as-prepared ZnO@ZIF-8 nanorod and nanotube arrays, respectively. (e) XRD patterns of ZnO@ZIF-8 nanorod arrays and nanotube arrays.

semiconductors with excellent photoelectric properties and is especially regarded as a promising candidate for photovoltaic and photocatalysis applications.[21] Under excitation of light (λ < 380 nm), ZnO can generate holes and electrons, and these photogenerated carriers recombine with each other, or migrate to surface trapping sites and react with redox species on the surface or in solution.[22] By combining with ZIF-8, which just has a small aperture of 3.4 Å, ZnO@ZIF-8 nanorod arrays should show different photocurrent responses for hole scavengers with various sizes. Herein, we take two reductive species, H_2O_2 and AA, as examples (see Scheme 2). As H_2O_2 is smaller than the pore apertures of ZIF-8, it can pass through the ZIF-8 pores and is oxidized by the photogenerated holes on the surface of ZnO nanorods ($H_2O_2 + 2h^+ \rightarrow 2H^+ + O_2$); meanwhile the photogenerated electrons are left and transported to the electrode substrate along the axial direction of ZnO nanorods, leading to great enhancement in the photocurrent response of ZnO nanorod arrays. On the contrary, AA cannot produce a similar enhancement effect to photocurrent response because its molecule size is larger than the pore aperture of ZIF-8.

To demonstrate this idea, we tested the PEC characteristics of ZnO nanorods arrays before and after coated ZIF-8 in the presence of different hole scavengers. Without ZIF-8, the photocurrent response (i.e., $\Delta I = I_{on} - I_{off}$) of the ZnO nanorod array can be markedly enhanced by the addition of both H_2O_2 and AA (Figure 6a). The enhancement effect of AA is larger than H_2O_2 because of its better ability to scavenge holes. After the nanorod arrays are coated with ZIF-8, the dark current (i.e., the baseline) is obviously decreased as shown in Figure 6b, indicating that the diffusion of H_2O onto the surface

dx.doi.org/10.1021/ja311085e | J. Am. Chem. Soc. 2013, 135, 1926−1933

Scheme 2. Schematic Diagram of the PEC Sensor with Selectivity to H_2O_2

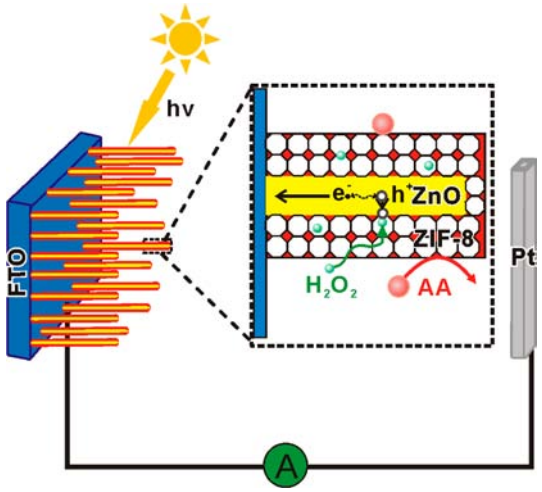

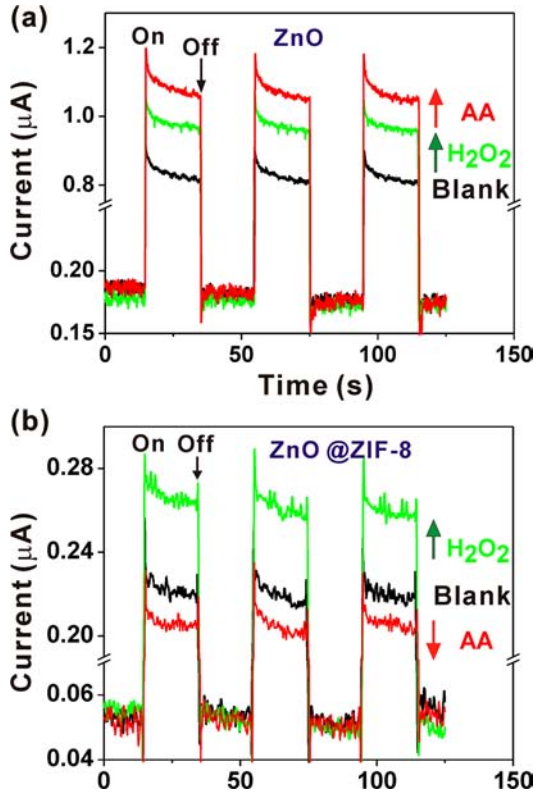

Figure 6. (a) Photocurrent response of ZnO nanorod arrays against H_2O_2 (0.1 mM) and AA (0.1 mM). (b) Photocurrent responses of the ZnO@ZIF-8 nanorod array in the presence of H_2O_2 (0.1 mM) and AA (0.1 mM).

of ZnO nanorods is greatly affected due to the presence of ZIF-8. This is because the diffusion of H_2O is greatly limited by the hydrophobicity of ZIF-8 although H_2O can enter into the pores of ZIF-8.[23] Interestingly, the photocurrent responses of the ZnO@ZIF-8 nanorod arrays display opposite changes with the addition of H_2O_2 or AA. The photocurrent response of the ZnO@ZIF-8 nanorod arrays is positively enhanced by the addition of H_2O_2, while the photocurrent response is markedly reduced by the addition of AA. Structurally, H_2O_2 is much smaller in size than the aperture of ZIF-8, so it is able to arrive in the ZnO surface through the shell of ZIF-8 and scavenge the photogenerated holes, leading to the enhancement of photocurrent response. As the molecule size of AA is larger than the aperture size of ZIF-8, the pores of ZIF-8 could be obstructed by AA. Therefore diffusion of H_2O that contributes to the photocurrent at blank situation is restrained, thereby resulting in the reduction of photocurrent response.

Notably, the photocurrent response of the ZnO@ZIF-8 nanorod array strongly depends on the concentration of hole scavengers added in the electrolyte solution. As shown in Figure 7a, the photocurrent response becomes larger and larger

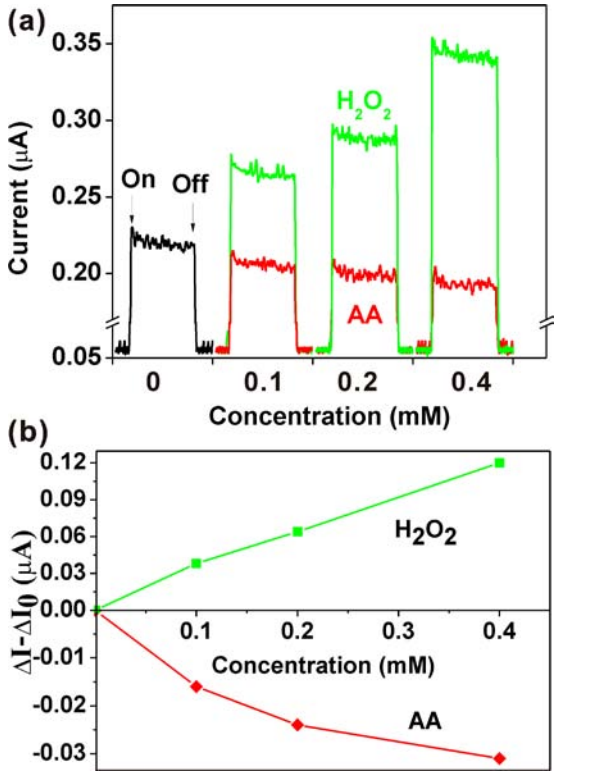

Figure 7. Photocurrent responses of the ZnO@ZIF-8 nanorod array in the presence of H_2O_2 and AA with different concentrations. (b) $\Delta I - \Delta I_0$ curves in the presence of H_2O_2 and AA with the concentrations as functions.

with the concentration of H_2O_2 added, whereas the photocurrent response decreases with the concentration of AA added. Figure 7b, in which the vertical ordinate is defined as $\Delta I - \Delta I_0$ (ΔI_0, the photocurrent response without adding any hole scavengers; ΔI, the photocurrent response in the presence of H_2O_2 or AA), quantitatively depicts the change of the photocurrent response of the ZnO@ZIF-8 nanorod array as a function of the concentration of hole scavengers. It can be clearly seen that such positive or negative influence of hole scavengers on the PEC response of ZnO@ZIF-8 nanorods is linear to the concentrations of hole scavengers within a certain range. This result indicates that the as-prepared ZnO@ZIF-8 nanorods array is potentially applied to PEC-based sensors.

It is well-known that as a basic metabolite of oxygen in a living system, overproduction of H_2O_2 can result in oxidative stress leading to progression of disease-related patho-physiological complications in many conditions.[24] Therefore the detection of H_2O_2 in a biosystem is very necessary. In our study, we primarily demonstrated that ZnO@ZIF-8 nanorod

dx.doi.org/10.1021/ja311085e | J. Am. Chem. Soc. 2013, 135, 1926−1933

arrays could detect H_2O_2 in the presence of serous buffer solution (Figure 8). Obviously, the photocurrent response $\Delta I(I_{on} - I_{off})$ becomes larger as the increase of H_2O_2 concentration with good linearity (Supporting Information, Figure S8).

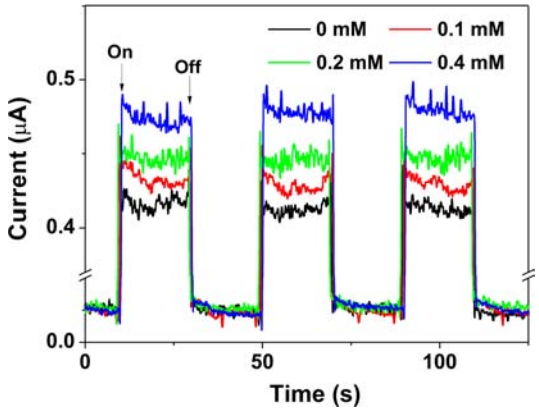

Figure 8. Photocurrent response curves of the ZnO@ZIF-8 nanorod arrays toward H_2O_2 with different concentrations in serous buffer solution.

4. CONCLUSIONS

ZnO@ZIF-8 nanorods with core−shell structures were successfully synthesized on the basis of a self-template strategy where ZnO nanorods not only act as the template but also provide Zn^{2+} ions for the formation of ZIF-8. Our experiments demonstrated that the solvent composition and reaction temperature are crucial for good control of the ZnO@ZIF-8 nanorods, as both of them have great influence on the balance between the dissolution rate of ZnO nanorods and the coordination rate of 2-methylimidazole with the released Zn^{2+} ions. Considering that ZnO possesses diverse nanomorphologies, more ZnO@ZIF-8 heterostructures and even hollow structures can be potentially obtained by means of similar synthetic methods. In this regard, our proposed self-template synthetic strategy opens a new pathway for fabricating MOFs-related core−shell heterostructures. More importantly, the as-prepared ZnO@ZIF-8 heterostructures presented selective PEC response toward different hole scavengers due to the presence of ZIF-8. We demonstrated that the ZnO@ZIF-8 nanorod arrays can be applied to the detection of H_2O_2 in serous buffer solution. Therefore such novel semiconductor@MOF core−shell heterostructures may be potentially developed into a new-type of photoelectrochemical sensors with molecule-size selectivity.

■ ASSOCIATED CONTENT

Supporting Information

SEM images, TEM images, and XRD patterns of freestanding ZnO nanorods, freestanding ZnO@ZIF-8 nanorods prepared under different reaction temperatures and mixed solvents, ZnO nanorod arrays, ZnO nanotube array, ZnO@ZIF-8 nanorod arrays, and ZnO@ZIF-8 nanotube arrays; SEM and XRD of the product obtained in mixed solution of DEF and H_2O; PEC measurement data for H_2O_2 detection in serous buffer solution. This material is available free of charge via the Internet at http://pubs.acs.org.

■ AUTHOR INFORMATION

Corresponding Author

qkuang@xmu.edu.cn; xjkong@xmu.edu.cn

Notes

The authors declare no competing financial interest.

■ ACKNOWLEDGMENTS

This work was supported by the National Basic Research Program of China (Grant Nos. 2011CBA00508), the National Natural Science Foundation of China (Grant Nos. 21021061, 21073145, 20901064, and 21171142), and the program for New Century Excellent Talents in University (NCET-11-0294).

■ REFERENCES

(1) (a) Jiang, H. L.; Xu, Q. *Chem. Commun.* **2011**, *47*, 3351−3370. (b) Rowsell, J. L. C.; Yaghi, O. M. *Microporous Mesoporous Mater.* **2004**, *73*, 3−14. (c) Tranchemontagne, D. J.; Mendoza-Cortes, J. L.; O'Keeffe, M.; Yaghi, O. M. *Chem. Soc. Rev.* **2009**, *38*, 1257−1283.

(2) (a) Achmann, S.; Hagen, G.; Kita, J.; Malkowsky, I.; Kiener, C.; Moos, R. *Sensors* **2009**, *9*, 1574−1589. (b) Chen, B.; Xiang, S.; Qian, G. *Acc. Chem. Res.* **2010**, *43*, 1115−1124. (c) Chen, B. L.; Wang, L. B.; Xiao, Y. Q.; Fronczek, F. R.; Xue, M.; Cui, Y. J.; Qian, G. D. *Angew. Chem., Int. Ed.* **2009**, *48*, 500−503. (d) Liu, S.; Xiang, Z. H.; Hu, Z.; Zheng, X. P.; Cao, D. P. *J. Mater. Chem.* **2011**, *21*, 6649−6653. (e) Lu, G.; Hupp, J. T. *J. Am. Chem. Soc.* **2010**, *132*, 7832−7833. (f) Ameloot, R.; Pandey, L.; Van, d. A. M.; Alaerts, L.; Sels, B. F.; De, V. D. E. *Chem. Commun.* **2010**, *46*, 3735−3737.

(3) (a) Jiang, H.-L.; Akita, T.; Ishida, T.; Haruta, M.; Xu, Q. *J. Am. Chem. Soc.* **2011**, *133*, 1304−1306. (b) Song, F.-J.; Wang, C.; Falkowski, J. M.; Ma, L. Q.; Lin, W. B. *J. Am. Chem. Soc.* **2010**, *132*, 15390−15398. (c) Tanabe, K. K.; Cohen, S. M. *Angew. Chem., Int. Ed.* **2009**, *48*, 7424−7427. (d) Tran, U. P. N.; Le, K. K. A.; Phan, N. T. S. *ACS Catal.* **2011**, *1*, 120−127.

(4) (a) Chen, B.; Liang, C.; Yang, J.; Contreras, D. S.; Clancy, Y. L.; Lobkovsky, E. B.; Yaghi, O. M.; Dai, S. *Angew. Chem., Int. Ed.* **2006**, *45*, 1390−1393. (b) Guo, H.; Zhu, G.; Hewitt, I. J.; Qiu, S. *J. Am. Chem. Soc.* **2009**, *131*, 1646−1647. (c) Venna, S. R.; Carreon, M. A. *J. Am. Chem. Soc.* **2010**, *132*, 76−78.

(5) (a) An, J.; Rosi, N. L. *J. Am. Chem. Soc.* **2010**, *132*, 5578−5579. (b) Cho, W.; Lee, H. J.; Oh, M. *J. Am. Chem. Soc.* **2008**, *130*, 16943−16946. (c) Furukawa, H.; Ko, N.; Go, Y. B.; Aratani, N.; Choi, S. B.; Choi, E.; Yazaydin, A. O.; Snurr, R. Q.; O'Keeffe, M.; Kim, J.; Yaghi, O. M. *Science* **2010**, *329*, 424−428. (d) Jeon, Y. M.; Armatas, G. S.; Heo, J.; Kanatzidis, M. G.; Mirkin, C. A. *Adv. Mater.* **2008**, *20*, 2105−2110. (e) Zheng, B.; Bai, J.; Duan, J.; Wojtas, L.; Zaworotko, M. J. *J. Am. Chem. Soc.* **2011**, *133*, 748−751.

(6) (a) Aijaz, A.; Karkamkar, A.; Choi, Y. J.; Tsumori, N.; Ronnebro, E.; Autrey, T.; Shioyama, H.; Xu, Q. *J. Am. Chem. Soc.* **2012**, *134*, 13926−13929. (b) Dhakshinamoorthy, A.; Garcia, H. *Chem. Soc. Rev.* **2012**, *41*, 5262−5284. (c) Gu, X.; Lu, Z. H.; Jiang, H. L.; Akita, T.; Xu, Q. *J. Am. Chem. Soc.* **2011**, *133*, 11822−11825. (d) Huang, Y.; Lin, Z.; Cao, R. *Chem.—Eur. J.* **2011**, *17*, 12706−12712. (e) Jiang, H. L.; Liu, B.; Akita, T.; Haruta, M.; Sakurai, H.; Xu, Q. *J. Am. Chem. Soc.* **2009**, *131*, 11302−11303. (f) Jiang, H. L.; Akita, T.; Ishida, T.; Haruta, M.; Xu, Q. *J. Am. Chem. Soc.* **2011**, *133*, 1304−1306. (g) Lu, G.; Li, S.; Guo, Z.; Farha, O. K.; Hauser, B. G.; Qi, X.; Wang, Y.; Wang, X.; Han, S.; Liu, X.; DuChene, J. S.; Zhang, H.; Zhang, Q.; Chen, X.; Ma, J.; Loo, S. C. J.; Wei, W. D.; Yang, Y.; Hupp, J. T.; Huo, F. *Nat. Chem.* **2012**, *4*, 310−316. (h) Pan, Y.; Yuan, B.; Li, Y.; He, D. *Chem. Commun.* **2010**, *46*, 2280−2282.

(7) (a) Esken, D.; Noei, H.; Wang, Y.; Wiktor, C.; Turner, S.; Van, T. G.; Fischer, R. A. *J. Mater. Chem.* **2011**, *21*, 5907−5915. (b) Esken, D.; Turner, S.; Wiktor, C.; Kalidindi, S. B.; Van, T. G.; Fischer, R. A. *J. Am. Chem. Soc.* **2011**, *133*, 16370−16373.

(8) (a) Lee, H. J.; Cho, W.; Oh, M. *Chem. Commun.* **2012**, *48*, 221−223. (b) Zhang, Y.; Lan, D.; Wang, Y.; Cao, H.; Jiang, H. *Phys. E* **2011**,

43, 1219−1223. (c) Shekhah, O.; Fu, L. L.; Sougrat, R.; Belmabkhout, Y.; Cairns, A. J.; Giannelis, E. P.; Eddaoudi, M. *Chem. Commun.* **2012**, *48*, 11434−11436. (d) Liu, N.; Yao, Y.; Cha, J.; McDowell, M.; Han, Y.; Cui, Y. *Nano Res.* **2012**, *5*, 109−116. (e) Yang, S. J.; Choi, J. Y.; Chae, H. K.; Cho, J. H.; Nahm, K. S.; Park, C. R. *Chem. Mater.* **2009**, *21*, 1893−1897. (f) Sorribas, S.; Zornoza, B.; Tellez, C.; Coronas, J. *Chem. Commun.* **2012**, *48*, 9388−9390.

(9) (a) Law, M.; Greene, L. E.; Johnson, J. C.; Saykally, R.; Yang, P. *Nat. Mater.* **2005**, *4*, 455−459. (b) Zhang, Q.; Dandeneau, C. S.; Zhou, X.; Cao, G. *Adv. Mater.* **2009**, *21*, 4087−4108.

(10) (a) Ke, F.; Qiu, L. G.; Yuan, Y.-P.; Jiang, X.; Zhu, J.-F. *J. Mater. Chem.* **2012**, *22*, 9497−9500. (b) Liu, N.; Yao, Y.; Cha, J.; McDowell, M.; Han, Y.; Cui, Y. *Nano Res.* **2012**, *5*, 109−116.

(11) (a) Reboul, J.; Furukawa, S.; Horike, N.; Tsotsalas, M.; Hirai, K.; Uehara, H.; Kondo, M.; Louvain, N.; Sakata, O.; Kitagawa, S. *Nat. Mater.* **2012**, *11*, 717−723. (b) Guo, H.; Zhu, G.; Hewitt, I. J.; Qiu, S. *J. Am. Chem. Soc.* **2009**, *131*, 1646−1647. (c) Li, R.; Yuan, Y. P.; Qiu, L. G.; Zhang, W.; Zhu, J. F. *Small* **2012**, *8*, 225−230. (d) Majano, G.; Perez Ramirez, J. *Adv. Mater.* **2012**, DOI: 10.1002/adma.201203664.

(12) (a) Han, X.; Zhou, X.; Jiang, Y.; Xie, Z. *J. Mater. Chem.* **2012**, *22*, 10924−10928. (b) Wang, Z. L. *J. Phys.: Condens. Matter* **2004**, *16*, R829−R858. (c) Wang, Z. L. *Mater. Today* **2004**, *7*, 26−33. (d) Zhou, X.; Xie, Z. X.; Jiang, Z. Y.; Kuang, Q.; Zhang, S.-H.; Xu, T.; Huang, R. B.; Zheng, L.-S. *Chem. Commun.* **2005**, 5572−5574.

(13) (a) Huang, X.; Lin, Y.; Zhang, J.; Chen, X. *Angew. Chem., Int. Ed.* **2006**, *45*, 1557−1559. (b) Li, H.; Eddaoudi, M.; O'Keeffe, M.; Yaghi, M. *Nature* **1999**, *402*, 276−279.

(14) Han, X. G.; Jiang, Y. Q.; Xie, S. F.; Kuang, Q.; Zhou, X.; Cai, D. P.; Xie, Z. X.; Zheng, L. S. *J. Phys. Chem. C* **2010**, *114*, 10114−10118.

(15) Guo, H.; Zhou, J.; Lin, Z. *Electrochem. Commun.* **2008**, *10*, 146−150.

(16) Guo, H. H.; Lin, Z. H.; Feng, Z. F.; Lin, L. L.; Zhou, J. Z. *J. Phys. Chem. C* **2009**, *113*, 12546−12550.

(17) Huang, X.; Lin, Y.; Zhang, J.; Chen, X. *Angew. Chem., Int. Ed.* **2006**, *45*, 1557−1559.

(18) (a) Cravillon, J.; Nayuk, R.; Springer, S.; Feldhoff, A.; Huber, K.; Wiebcke, M. *Chem. Mater.* **2011**, *23*, 2130−2141. (b) Pan, Y.; Heryadi, D.; Zhou, F.; Zhao, L.; Lestari, G.; Su, H.; Lai, Z. *CrystEngComm* **2011**, *13*, 6937−6940. (c) Pan, Y.; Liu, Y.; Zeng, G.; Zhao, L.; Lai, Z. *Chem. Commun.* **2011**, *47*, 2071−2073. (d) Venna, S. R.; Jasinski, J. B.; Carreon, M. A. *J. Am. Chem. Soc.* **2010**, *132*, 18030−18033.

(19) Shi, Q.; Chen, Z.; Song, Z.; Li, J.; Dong, J. *Angew. Chem., Int. Ed.* **2011**, *50*, 672−675.

(20) (a) Kuang, Q.; Xu, T.; Xie, Z. X.; Lin, S. C.; Huang, R. B.; Zheng, L. S. *J. Mater. Chem.* **2009**, *19*, 1019−1023. (b) Remias, R.; Kukovecz, A.; Daranyi, M.; Kozma, G.; Varga, S.; Konya, Z.; Kiricsi, I. *Eur. J. Inorg. Chem.* **2009**, 3622−3627.

(21) (a) Cho, H. D.; Zakirov, A. S.; Yuldashev, S. U.; Ahn, C. W.; Yeo, Y. K.; Kang, T. W. *Nanotechnology* **2011**, *23*, 115401. (b) Kakiuchi, K.; Hosono, E.; Fujihara, S. *J. Photochem. Photobiol. A* **2006**, *179*, 81−86. (c) Yang, X.; Wolcott, A.; Wang, G.; Sobo, A.; Fitzmorris, R. C.; Qian, F.; Zhang, J. Z.; Li, Y. *Nano Lett.* **2009**, *9*, 2331−2336.

(22) (a) Dotan, H.; Sivula, K.; Gratzel, M.; Rothschild, A.; Warren, S. C. *Energy Environ. Sci.* **2011**, *4*, 958−964. (b) Gan, J.; Lu, X.; Zhai, T.; Zhao, Y.; Xie, S.; Mao, Y.; Zhang, Y.; Yang, Y.; Tong, Y. *J. Mater. Chem.* **2011**, *21*, 14685−14692. (c) Qiu, Y.; Yan, K.; Deng, H.; Yang, S. *Nano Lett.* **2012**, *12*, 407−413.

(23) Mu, L.; Liu, B.; Liu, H.; Yang, Y.; Sun, C.; Chen, G. *J. Mater. Chem.* **2012**, *22*, 12246−12252.

(24) (a) Karyakin, A. A.; Puganova, E. A.; Budashov, I. A.; Kurochkin, I. N.; Karyakina, E. E.; Levchenko, V. A.; Matveyenko, V. N.; Varfolomeyev, S. D. *Anal. Chem.* **2004**, *76*, 474. (b) Albers, A. E.; Okreglak, V. S.; Chang, C. J. *J. Am. Chem. Soc.* **2006**, *128*, 9640−9641.